

Spatiotemporal Dynamics of the Slow Oscillation in a Thalamocortical Network Model

Jason S. Sherfey

Abstract

Rhythmicity is a ubiquitous feature of neural activity that results from an interaction between intrinsic currents and extrinsic network properties. The most prominent rhythm during sleep appears in extracranial EEG as a large amplitude, ~ 1 Hz Slow Oscillation (SO) with $\sim 10,000$ cycles per night. SO is known to orchestrate activity across the cortex during slow-wave sleep and may be involved in important restorative functions and memory consolidation. Understanding the biophysical basis and spatiotemporal dynamics of the oscillation would provide direct insight into fundamental aspects of sleep function. Conflicting evidence from animal and human studies with different recording techniques has produced multiple theories that have yet to be resolved. One question that must be answered for this research to advance is does the SO occur synchronously or propagate across the cortex, and what are the underlying mechanisms governing the dynamics? To address the question of potential generating mechanisms, I studied a thalamocortical network model of the SO and developed an approach to model specification that facilitates model comparison.

1 Introduction

The Slow Oscillation (SO) is a fundamental cortical operating mode of NREM sleep. SO consists of a DOWN state with a strong outward potassium current in layers 2/3, decreased broadband gamma activity, and very low firing, alternating at ~ 1 Hz with an UP state when most cells fire at near waking levels (see Figure 1). Rhythmicity can arise in many ways including the interaction of activation and inactivation time-constants between different ion channels, even in the absence of synaptic input [1], or from the delays in excitatory and inhibitory feedback in local networks. Electrical coupling may play an important role in fast rhythms [2]. Within the thalamus, cells of the nucleus reticularis (RE) provide inhibitory feedback to thalamocortical (TC) cells [3]. Widespread cholinergic and GABAergic cortical projects from the nucleus basalis have been shown in rats to exert an important influence on EEG rhythms [4]. In general, evidence suggests rhythms emerge as a result of mutually-reinforcing interactions between intrinsic currents, local circuits, and distant pacemakers [3].

It has been claimed, based on referential scalp EEG that sleep SO begins focally and then spreads through the cortex at a rate of $\sim 2-7$ m/s [5]. SO during NREM sleep travels across the cortex in cats [6], and over the scalp in humans, with the originating site related to pre-sleep experience [5]. This has been taken as evidence for a possibly organized replay of daytime experience during sleep for the purposes of memory consolidation. However, recent MEG and intracranial macroelectrode and microelectrode recordings have revealed that the dynamics are more complicated in humans. Isolated DOWN states have been found to occur, and DOWN states may be more frequent than UP states [7]. Furthermore, recent evidence suggests that special cell populations may act as hubs triggering SO and linking SO activity between cortical regions [8].

We analyzed MEG and EEG from healthy subjects during natural sleep and intracranial electrical recordings from patients with epilepsy undergoing invasive monitoring of seizure foci prior to their surgical removal. The MEG and EEG data displayed both SOs propagating from focal origins and others occurring synchronously across large regions of cortex. Preliminary intracranial recordings of cortical population activity have shown similar patterns. These observations have led to the hypothesis that there may be two synchronizing mechanisms, one thalamo-cortical (for synchronous SO) and the other cortico-cortical (for travelling SO). In order to better understand potential mechanisms, we present here simulation results from a model of a cortico-cortical mechanism ([9], [10], [11]), potential thalamo-cortical mechanisms, and propose a modeling and simulation strategy for addressing the question of how these generating mechanisms relate to each other and for advancing slow oscillation research, in general.

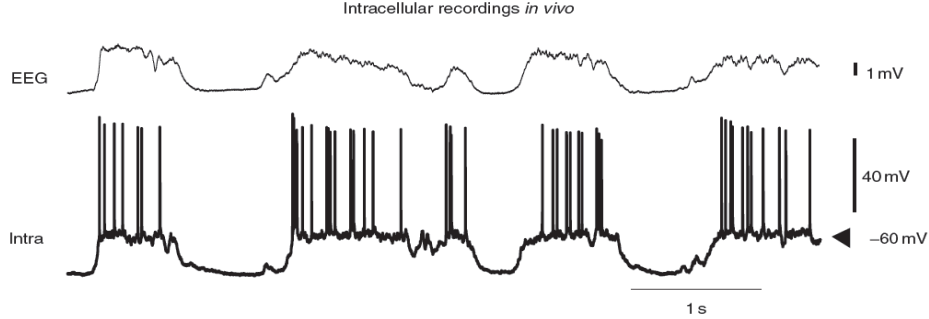


Figure 1. The slow oscillation in intracellular and EEG recordings [8].

2 Methods

2.1 Experimental data analysis

We recorded MEG, EEG, and intracranial EEG in humans during slow wave sleep and quantified the spatiotemporal activity patterns of all SO cycles. The instantaneous phase of the narrow band-pass filtered signal (.1-2Hz) was used to automatically detect slow oscillations during NREM stages 3 and 4. The correlation between distance and propagation delay between all sensor pairs was calculated for each SO. Correlation coefficients and delay maps summarized spatiotemporal characteristics of SO propagation.

2.2 Thalamocortical model of the slow oscillation

We simulated a thalamocortical network model [9] capable of generating two common sleep rhythms, sleep spindles and slow oscillations [12]. The network model consisted of single-compartment models of thalamocortical (TC) and thalamic reticular (RE) cells as well as two-compartment models of cortical interneurons (IN) and pyramidal (PY) cells.

The thalamic model (TC, RE) contained ion channels described by Hodgkin-Huxley kinetics:

$$C_m \frac{dV}{dt} = -g_L(V - E_L) - I^{int} - I^{syn}$$

where $C_m = 1 \mu\text{F}/\text{cm}^2$ is the membrane capacitance, g_L is the leak conductance, and E_L is the reversal potential. I^{int} is the sum of intrinsic currents: $I_{Na(t)}$, I_K , I_{TS} , and I_{KL} in RE cells and $I_{Na(t)}$, I_K , I_T , I_{KL} , I_h and I_A in TC cells (see Figure 2). Parameter values and expressions for the voltage- and calcium-dependent currents are given in the Supplementary section. I^{syn} is the sum of synaptic currents (see Figure 3).

The cortical model (PY, IN) consisted of dendritic and axosomatic compartments containing ion channels described by Hodgkin-Huxley kinetics:

$$C_m \frac{dV_D}{dt} = -g_L(V_D - E_L) - g(V_D - V_S) - I_D^{int} - I^{syn}$$

$$C_m \frac{dV_S}{dt} = -g_L(V_S - E_L) - g(V_S - V_D) - I_S^{int} - I^{syn}$$

where C_m , g_L , and E_L are the same in both compartments. V_D and V_S are the membrane potentials of the dendritic and axosomatic compartments, respectively. I_D^{int} is the sum of intrinsic, dendritic currents: $I_{Na(t)}$, I_{KL} , $I_{Na(p)}$, I_{K_m} , I_{KCa} , and I_{HVA} in PY cells. I_S^{int} is the sum of intrinsic, axosomatic currents: $I_{Na(t)}$, I_K , and $I_{Na(p)}$ in PY cells. IN cells have the same intrinsic currents as PY cells except for the persistent sodium current, $I_{Na(p)}$. The strength of coupling between the two compartments is determined by $g = \frac{1}{\kappa * S_{dend}}$ where $S_{dend} = S_{soma} * \rho$, $\kappa = 1E4$, and $\rho = 165$ (PY) or 50 (IN).

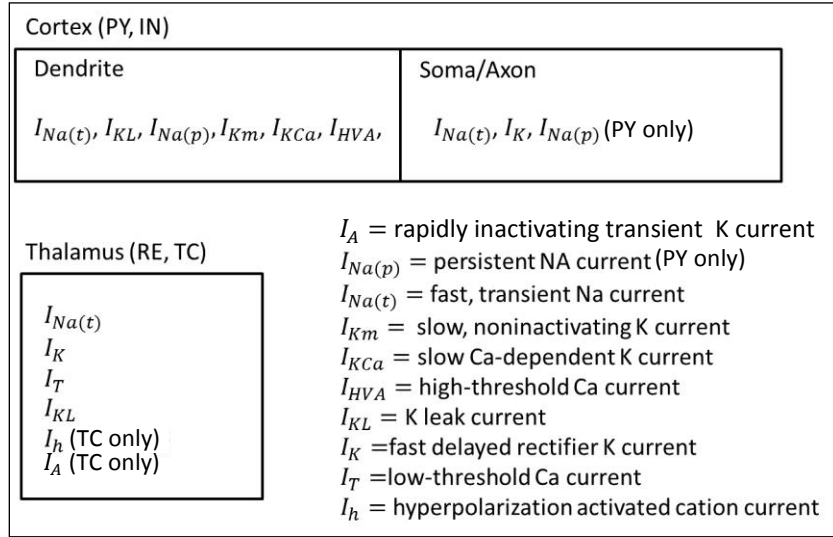


Figure 2. Intrinsic currents in thalamocortical SO model.

Cells were connected by excitatory (*AMPA*, *NMDA*) and inhibitory (*GABA_A*) synapses described by first-order activation kinetics and calculated by

$$I^{syn} = g_{syn}[O](V - E_{syn})$$

where g_{syn} is the maximal conductivity, $[O](t)$ is the fraction of open channels, and E_{syn} is the reversal potential. All synapses were capable of experiencing "synaptic fatigue" with sustained activation and produced spontaneous, miniature postsynaptic potentials (EPSPs or IPSPs). Synaptic fatigue was modeled by multiplying the conductance by an activity-dependent scaling parameter, $D \in [0,1]$, representing available synaptic resources:

$$I^{syn} = D * g_{syn}[O](V - E_{syn}).$$

D decreased with repetitive presynaptic firing according to $D = 1 - (1 - D_i(1 - U))e^{(-\frac{t-t_i}{\tau})}$

where $U = 0.07$ = fraction of resources used per action potential, $\tau = 700ms$ = time constant of the recovery of synaptic resources, D_i = value of D immediately before the i^{th} event at time t_i . Spontaneous PSPs had small amplitudes, the same kinetics as spike-triggered PSPs, and occurred at random times modeled by a Poisson process with a mean rate of $\mu(t) = \log\left(\frac{t-t_0+\tau}{\tau}\right) \frac{1}{400}$ where t_0 = time of last presynaptic spike and $\tau = 50$. The network connectivity matrix was defined by specifying "fanouts" between cell types. Each cell was assigned a position in 1-D. A cell of type A at position X connected to all cells of type B located on the interval $X \pm F$ where F is the fanout from cell type A to cell type B.

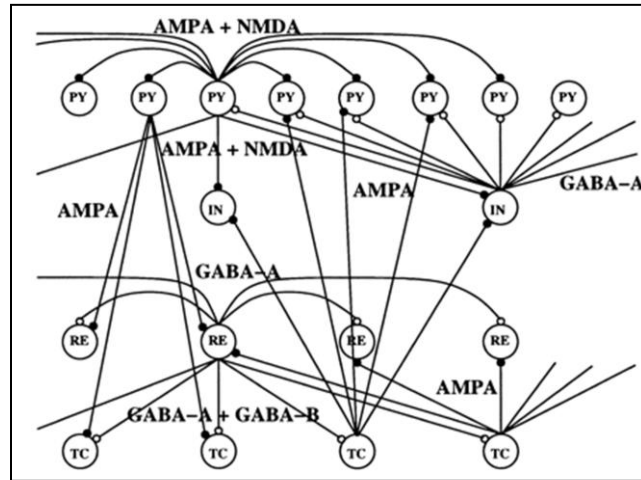


Figure 3. Synaptic connectivity in thalamocortical SO model. [9].

3 Results

3.1 Spatiotemporal characteristics of sleep SO in MEG and EEG

Individual slow oscillations can appear synchronously across broadly distributed channels in EEG (Figure 4, B1) and simultaneous MEG (Figure 4, B2) or with a delay between channels (Figure 4, B3 & B4). A SO delay map can be constructed by projecting sensor locations onto a plane and then interpolating the delay in SO detection time between channels. The EEG delay map for some SO strongly suggests that the SO has a focal origin and propagates uniformly across the cortex (Figure 4, A3). The simultaneous MEG delay map often shows a similar trend, though the EEG gradient is typically smoother than in the MEG. A SO traveling wave pattern produces a linear relationship between propagation delay and distance that is stronger in EEG (Figure 4, D3) than MEG (Figure 4, D4). At other times, the SO is synchronous across channels (Figure 4, B1 & B2) with a flat delay map (Figure 4, A1 & A2), and no relationship between propagation delay and distance (Figure 4, D1 & D2).

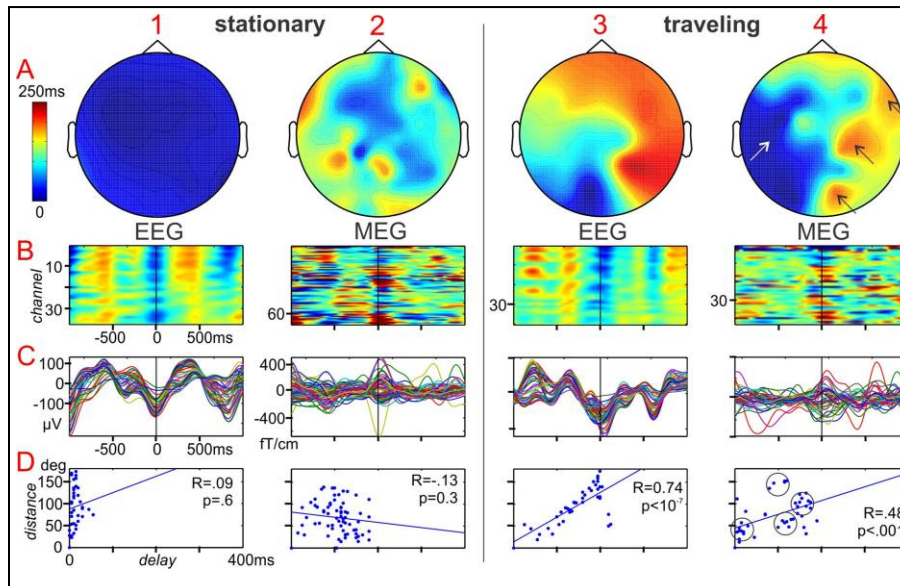


Figure 4. EEG and MEG evidence that the slow oscillation can be traveling or stationary.

3.2 Cellular and network mechanisms of SO activity

Intrinsic currents in thalamic neurons: both RE and TC cells contain fast sodium and fast, delayed potassium currents capable of generating Hodgkin-Huxley-type spikes (Figure 5, top). Also present in both cell types is a low-threshold calcium current, I_T , that flows inward upon activation and gives rise to low-threshold calcium-dependent spikes (LTS). I_T is a slowly inactivating current with a calcium concentration-dependent reversal potential that progressively hyperpolarizes the cell. Thus, LTSs triggered by I_T cause progressive hyperpolarization which gives rise to more LTSs. This dynamic underlies the augmenting response [13] in Figure 5 (NaK+iT). I_T -mediated LTSs can trigger $I_{Na(t)}$ spikes from more hyperpolarized states than otherwise possible. TC cells contain an additional depolarizing current I_h that is activated by hyperpolarization. Consequently, I_h can function as a pacemaker current, for instance, giving rise to the periodicity of rhythmic sleep spindles [14], and the periodic firing in Figure 5 (lower plots) where the simulation began in a hyperpolarized state.

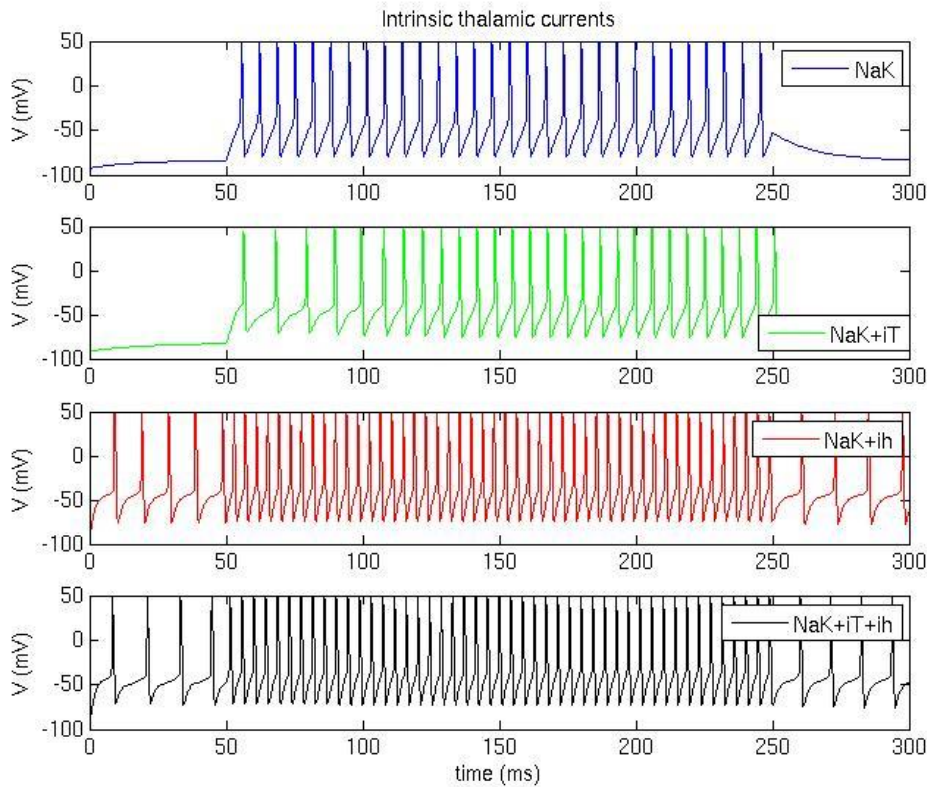


Figure 5. The effect of intrinsic currents on membrane potential dynamics. $I_{ext} = 10 \mu A/cm^2$.

Intrinsic currents in cortical neurons: both the dendritic and axosomatic compartments contain very fast Hodgkin-Huxley type sodium and potassium currents, $I_{Na(t)}$ and I_K , respectively, with a much greater density in the soma. Both compartments also contain a persistent sodium current, $I_{Na(p)}$. Slow calcium- and voltage-dependent dendritic currents (I_{K_m} , $I_{K_{Ca}}$) produce spike after-hyperpolarizations (AHPs) that underlie the low firing rate in Figure 6 (bottom). On the other hand, the high-voltage dendritic calcium current I_{HVA} contributes to after-depolarizations (ADPs), indirectly, by its modulatory effects on I_{K_m} and $I_{K_{Ca}}$ and, directly, by calcium influx. The long depolarization phase of the somatic action potential in Figure 6 is the result of $I_{Na(p)}$ and ADPs. The contribution of AHPs to firing rate and ADPs to the depolarization phase depends on the coupling strength, ρ , between

compartments [15]. Decreasing ρ eliminates the ADP which is most prominent in Figure 8a where $\rho = 165$ in PY cells and 50 in IN cells.

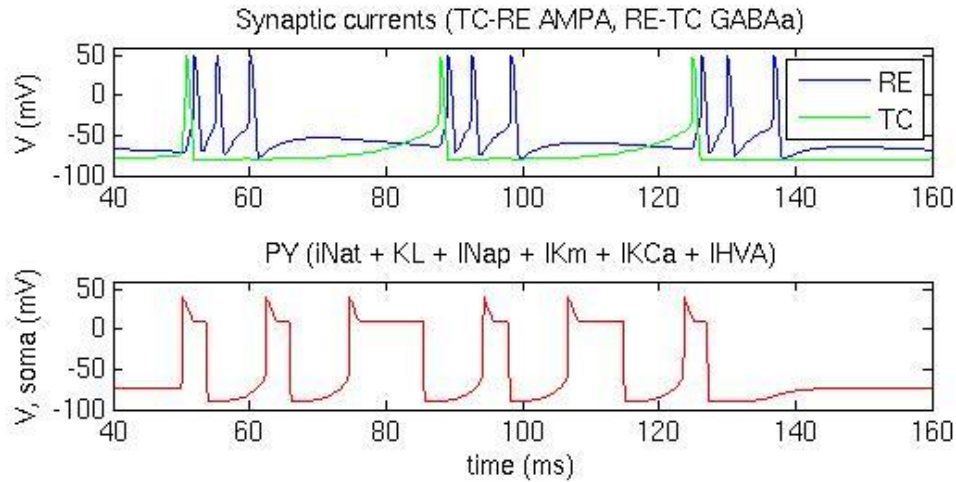


Figure 6. Thalamic connections and intrinsic currents in the cortical model. $I_{ext} = 10\mu A/cm^2$.

Thalamic networks: RE cells project inhibitory signals to neighboring RE cells and TC cells at $GABA_A$ synapses while TC cells reciprocally excite RE cells at $AMPA$ synapses. In a minimal model with one RE cell and one TC cell with steady external stimulation (Figure 6, top), a single TC spike triggers a reciprocal RE spike that sufficiently inhibits TC to mask the external stimulation and temporarily stop TC firing. I_T inactivates much more slowly in the RE cell and gives rise to spike triplets. I_T produces a small augmenting response during each RE spike triplet. Without excitation, I_T inactivation ends RE firing and enables TC to become sufficiently depolarized by external stimulation for the sequence to start over. $AMPA$ and $GABA_A$ synapses produce spontaneous, miniature EPSPs and IPSPs, respectively. The miniature IPSPs may contribute to the variability in the timing of the third spike in each triplet. In RE cells, I_T leads to long-duration LTSs that result in prolonged periods of $GABA_A$ release onto TC cells. When the inhibitory RE signal is decreased, the induced TC hyperpolarization promotes LTSs in TC cells and sufficiently activates I_h to produce subsequent TC spikes. That is, I_h provides the potential for rhythmic burst generation due to the GABA/AMPA currents in RE-TC circuits. A similar interaction is responsible for generating spindle oscillations and may be involved in SO dynamics as well.

Thalamocortical networks: all connections in the thalamocortical model are given in Figure 3 and exhibit synaptic fatigue and generate spontaneous PSPs. Figure 7 displays results from simulations of a network with the minimum number of cells and connections that include all types of cells and synapses. Only PY cells are stimulated by a steady external current $I_{ext} = 10\mu A/cm^2$. The effects of synaptic fatigue become evident under these conditions as the progressive decrease in RE firing rate reflects progressive depression of the PY-RE $AMPA$ conductance.

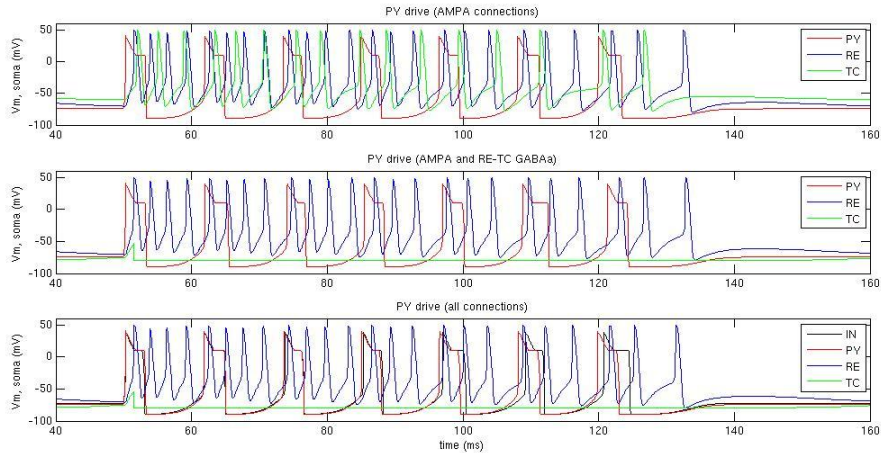


Figure 7. Simple thalamocortical networks with excitatory and inhibitory connections.

3.3 Network mechanisms of SO propagation

The thalamocortical models motivating the model presented here were developed to study potential mechanisms of traveling SO ([9], [10], [11]). In this section, we consider mechanisms of SO propagation before turning to potential mechanisms of synchronous SO. Supplementary Table 1 and Supplementary Table 2 display the cell populations and non-default parameter values used to produce the results in Figure 8.

In the original model, the SO begins with an UP state initiated by spontaneous mini-EPSPs that activate dendritic $I_{Na(p)}$ in sufficiently depolarized cells, triggering axosomatic spikes that propagate across cortex along excitatory cortico-cortical connections. Although spontaneous mini-EPSPs were present at AMPA synapses between PY cells, the number of cells and the EPSP amplitudes were too small in this simulation study to produce spikes reliably during short simulations. Consequently, in order to explore propagation patterns, I applied a short current pulse large enough to trigger bursting in a single PY neuron, mimicking the effect of a spontaneously generated spike.

Two 3-sec simulations with 45 cells were performed to test the effect of blocking $GABA_A$ conductance between IN and PY cells. In both cases, large ADPs are produced by the dendritic sodium and calcium currents in PY cells with strongly coupled dendritic and axosomatic compartments. Also, in both cases, the UP state propagates across the cortical network along cortico-cortical pathways. In the control case, the propagation is slow with a significant delay. When the $GABA_A$ conductance is blocked, the UP state appears nearly synchronous. However, instead of broadly distributed cortical cells being simultaneously driven and synchronously activated, the UP state is merely propagating much faster. Eliminating inhibition from interneurons has the effect of increasing cortico-cortical throughput; it is not a synchronizing mechanism. These results are consistent with experimental findings and simulation results obtained using a different model [10].

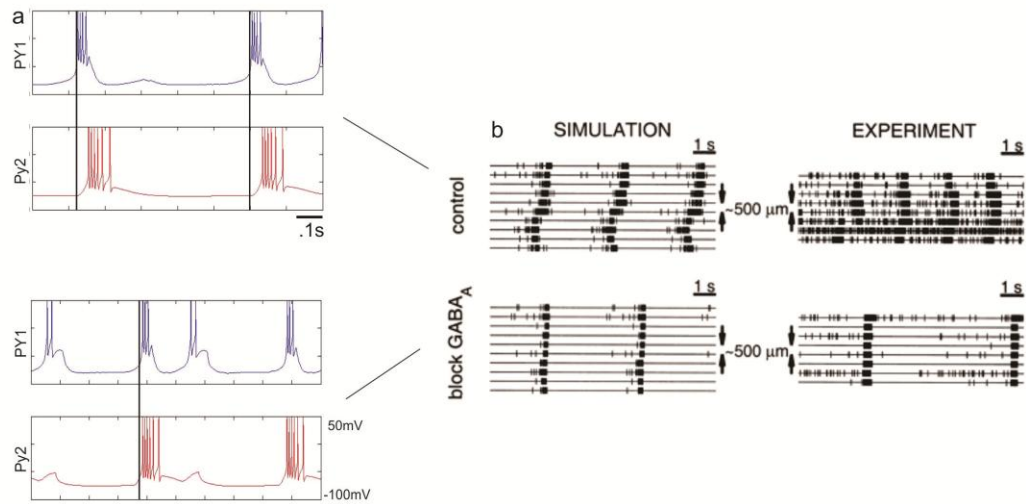


Figure 8. Comparison of (a) thalamocortical network model with (b) published results [10].

3.4 Synchronous slow oscillations

The model examined thus far accounts for key aspects of propagating SO but does not explain synchronous SO or SO that start with a DOWN state. In the remainder, we will consider potential mechanisms for synchronous SO that begin with a DOWN state.

The simplest potential generator of a synchronous DOWN state is widespread, synchronous inhibition. Two questions that follow immediately are (1) what causes synchronous inhibition, and (2) what drives the UP state after a synchronous DOWN state? We hypothesize that a trigger zone exists from which a relatively focal excitatory process drives a more distributed inhibitory process which gives rise to synchronous cortical inhibition. Secondly, we hypothesize that the UP state is a secondary phenomenon arising from the kinetics of recovery in previously inhibited cortical cells. This hypothesis was inspired, in part, by our observation in MEG data that DOWN states are more common and more frequently synchronous than UP states. Two cells with the same recovery kinetics would recover from synchronous inhibition simultaneously, whereas, variation in recovery kinetics across a cortical population would result in different spatiotemporal patterns of UP state onsets.

The thalamocortical model can be used to test hypotheses in at least two ways: (1) biophysical and network parameters can be varied, and (2) cell types and biophysical mechanisms can be added or removed. The first approach included testing the effects of varying TC-IN & IN-PY fanouts and $GABA_A$ conductances in order to study the effects of varying inhibition in the model. In all cases, effects were limited to varying propagation rate, durations of UP and DOWN states, or silencing the network. The second approach will be addressed in the Discussion below.

4 Discussion

Electrophysiological experiments, lesion studies and modeling studies have determined that interactions between synaptic currents ($GABA_A$, $AMPA$) and intrinsic currents (I_h , I_T) in thalamic neurons generate sleep spindles. Similar studies have demonstrated that excitatory interactions between cortical neurons, inhibitory feedback from interneurons, and intrinsic cortical currents ($I_{Na(p)}$, I_{HVA} , I_{Km} , I_{KCa}) are capable of generating SO. However, while the SO studies reveal an intrinsic rhythmicity which contributes to the SO, they do not account

for SO which are synchronous across the cortical surface, nor do they exclude a significant role of afferents extrinsic to the cortex in the natural SO.

Testing hypothesized mechanisms of synchronous SO which begin with a DOWN state using modeling and simulation will require implementing many variations on the model presented here. Results from animal and human studies implicate different cells in the generation and propagation of SO and different theories often involve different circuits. In addition, a wide range of intrinsic currents and biophysical mechanisms have been proposed to be involved. Only a very small subset of the space of potentially correct models has been implemented. These observations point to the need for an efficient method of designing, implementing, simulating, and comparing alternative models testing likely hypotheses. For instance, a more direct test of a hypothesized region that triggers widespread, synchronous inhibition would add a population to the current model and explore the effects of projecting onto TC cells exciting interneurons (trigger DOWN state by GABA inhibition) versus projecting onto RE cells inhibiting TC cells (trigger DOWN state by removing AMPA excitation). A modification like that is complicated by the fact that candidate trigger zones include different cortical layers and different cortical regions, suggesting that multiple cell types and associated biophysical mechanisms should be tested and the results compared.

The NEURON simulation environment [16] facilitates a similar kind of model flexibility at the single cell level. However, the same features which enable modeling almost any biophysical mechanism in space and time also make it difficult to scale up to small networks of neurons while maintaining the same degree of flexibility. I implemented the thalamocortical SO model in Matlab using a method motivated by NEURON's abstraction for handling biophysical mechanisms. The implementation enables biophysical mechanisms to be defined generically and then "inserted" into cells. Cells are then defined in terms of the biophysical mechanisms contained by them and a set of passive parameters. The present version of the thalamocortical simulator processes a spreadsheet used to define cells by providing such information and for specifying network connectivity (Supplementary Tables 1 and 2 were processed by the simulator to produce the above results).

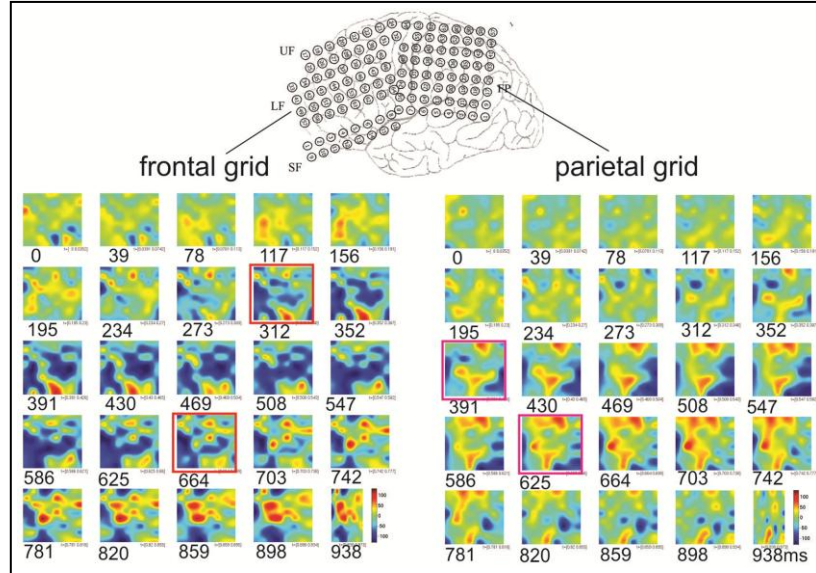
The next step in developing the simulator for efficient model construction will be to encapsulate network model definition and parameter specification in a program with a graphical interface designed to provide maximal flexibility, efficiency, and easy access to model parameters and equations (see Supplementary Figure 3). Also, the current Matlab implementation significantly limits the model size that can be simulated in a reasonable amount of time, and future modeling efforts will need to utilize a more efficient language like C++. Modeling the neural circuitry underlying SO will benefit from model comparison and better guide experimentation and interpretation toward an understanding of the biological neural mechanisms.

References

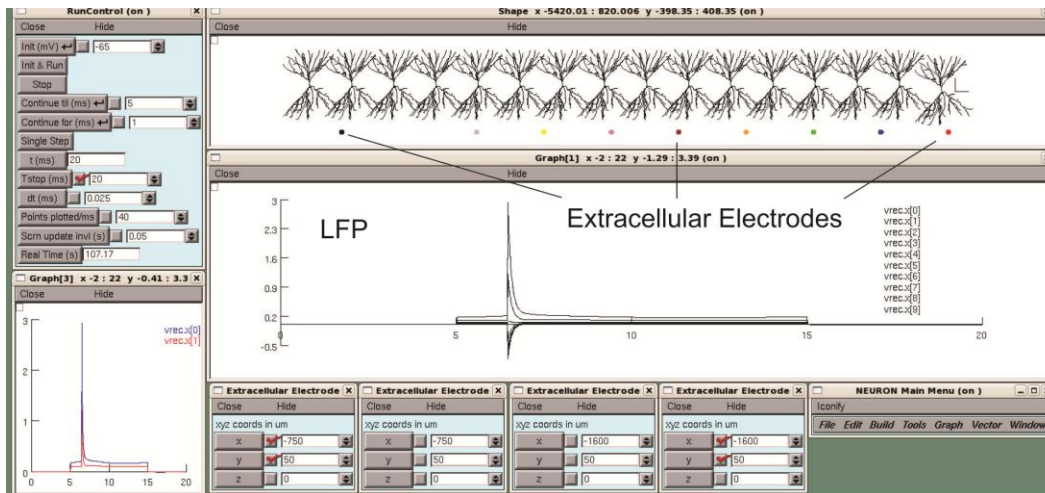
- [1] Llinas, R., The intrinsic electrophysiological properties of mammalian neurons: insights into central nervous system function. *Science*, 1988. 242(4886): p. 1654-64.
- [2] Traub, R.D., et al., Cellular mechanisms of neuronal population oscillations in the hippocampus in vitro. *Annu Rev Neurosci*, 2004. 27: p. 247-78.
- [3] Destexhe, A. and T.J. Sejnowski, Interactions between membrane conductances underlying thalamocortical slow-wave oscillations. *Physiol Rev*, 2003. 83(4): p. 1401-53.
- [4] Buzsaki, G., et al., Nucleus basalis and thalamic control of neocortical activity in the freely moving rat. *J Neurosci*, 1988. 8(11): p. 4007-26.
- [5] Massimini, M., et al., The sleep slow oscillation as a traveling wave. *J Neurosci*, 2004. 24(31): p. 6862-70.
- [6] Amzica, F. and M. Steriade, Short- and long-range neuronal synchronization of the slow (1 Hz) cortical oscillation. *J Neurophysiol*, 1995. 73(1): p. 20-38.
- [7] Cash, S.S., et al., The human K-complex represents an isolated cortical down-state. *Science*, 2009. 324(5930): p. 1084-7.

- [8] Destexhe, A., Spatiotemporal aspects of slow-waves and seizures in humans. *Brain*, 2010. 133(9): p. 2514-5.
- [9] Bazhenov, M., et al., Model of thalamocortical slow-wave sleep oscillations and transitions to activated States. *J Neurosci*, 2002. 22(19): p. 8691-704.
- [10] Sanchez-Vives, M.V. and D.A. McCormick, Cellular and network mechanisms of rhythmic recurrent activity in neocortex. *Nat Neurosci*, 2000. 3(10): p. 1027-34.
- [11] Traub, R.D., et al., Single-column thalamocortical network model exhibiting gamma oscillations, sleep spindles, and epileptogenic bursts. *J Neurophysiol*, 2005. 93(4): p. 2194-232.
- [12] Steriade, M., A. Nunez, and F. Amzica, Intracellular analysis of relations between the slow (1 Hz) neocortical oscillation and other sleep rhythms of the electroencephalogram. *J Neurosci*, 1993. 13(8): p. 3266-83.
- [13] Maxim Bazhenov (1998). Cellular and network models for intrathalamic augmenting responses during 10Hz stimulation. *J Neurophysiol* 79:2730-2748.
- [14] John Huguenard (1992). Simulation of the currents involved in rhythmic oscillations in thalamic relay neurons. *J Neurophysiol* 68(4).
- [15] Zacary Mainen (1996). Influence of dendritic structure on firing pattern in model neocortical neurons. *Nature* 382.
- [16] Hines, M.L. and Carnevale, N.T. NEURON: a tool for neuroscientists. *The Neuroscientist* 7:123-135, 2001.
- [17] Delorme, A. and S. Makeig, EEGLAB: an open source toolbox for analysis of single-trial EEG dynamics including independent component analysis. *Journal of Neuroscience Methods*, 2004. 134: p. 9-21.

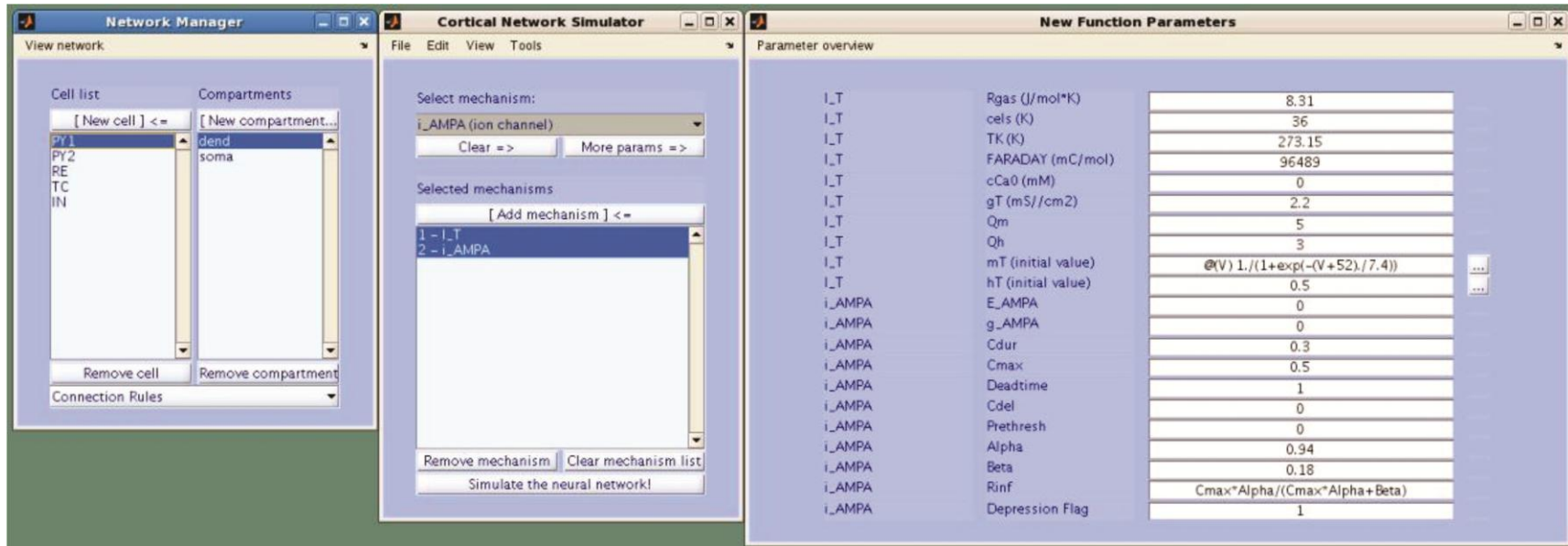
Supplementary Figures



Supplementary Figure 1: ECoG evidence for SO as a stationary wave.



Supplementary Figure 2. NEURON model including LFP calculations and cellular morphology.



Supplementary Figure 3: A potential interface for the Thalamocortical Network Simulator.

Program features:

- Hover over parameter names to display tooltips with the equation(s) containing the parameters (see middle column of the parameter window)
- Edit the ODEs defining the dynamics of state variables by clicking on the button next to the text box with their initial values (see mT, hT)
- Specify initial values using anonymous Matlab functions or constant values (see mT, hT)
- Specify any values using equations constructed out of other parameters defined for the same mechanism (see Rinf)
- Automatically store models, organizes results, and manage cluster computing

Supplementary Table 1: Four examples of the spreadsheet format for defining cell populations in the Thalamocortical Network Simulator.

Ex)	Cell	N	Intrinsic currents	Other mechanisms	Parameters	Values	Section
A	RE	1	{'iNaK'}		{'stim' 'S_RE' 'g_kl'}	[10 1.3E-4 .018]	
B	RE	1	{'iNaK' 'iTs'}		{'stim' 'S_RE' 'g_kl'}	[10 1.3E-4 .018]	
C	RE	1	{'iNaK' 'iTs'}		{'stim' 'S_RE' 'g_kl'}	[0 1.3E-4 .018]	
	TC	1	{'iA' 'iNaK' 'iT' 'ih'}	{'CaDecay'}	{'stim' 'S_TC' 'g_kl'}	[10 2.9E-4 .012]	
D	RE	1	{'iNaK' 'iTs'}		{'stim' 'S_RE' 'g_kl'}	[0 1.3E-4 .018]	
	TC	1	{'iA' 'iNaK' 'iT' 'ih'}	{'CaDecay'}	{'stim' 'S_TC' 'g_kl'}	[10 2.9E-4 .012]	
	PY	1	{'iCa' 'iKCa' 'iKm' 'iKv' 'iNap' 'iNav'}	{'CaDecay'}	{'stim' 'S_PY' 'g_kl' 'rho'}	[10 1.65e-4 15 165]	dend
	PY	1	{'iKv' 'iNap' 'iNav'}		{'stim' 'S_PY' 'g_kl' 'rho'}	[0 1.65e-4 165]	soma
	IN	1	{'iCa' 'iKCa' 'iKm' 'iKv' 'iNav'}	{'CaDecay'}	{'stim' 'S_IN' 'g_kl' 'rho'}	[0 1.65e-4 .8 50]	dend
	IN	1	{'iKv' 'iNav'}		{'stim' 'S_IN' 'g_kl' 'rho'}	[0 1.65e-4 0 50]	soma

Parameters: 'S_X' for scaling conductances, 'rho' for linking compartments, 'stim' for external stimulation, 'g_kl' for potassium leak conductance.

Supplementary Table 2: Fanout and synapse specification for $n = 5$

where #IN = n , #RE = #TC = $2n$ and #PY = $4n$.

Ex)		<i>postsynaptic</i>					<i>postsynaptic</i>			
D	Fanout	PY	IN	RE	TC	Synapse	PY	IN	RE	TC
<i>presynaptic</i>	PY	5	1	5	5	PY	AMPA, NMDA	AMPA, NMDA	AMPA	AMPA
	IN	5	0	0	0	IN	GABA _A			
	RE	0	0	5	5	RE			GABA _A	GABA _A
	TC	10	2	5	0	TC	AMPA	AMPA	AMPA	

Supplementary expressions:

iT

```
iT = @(V,m,h,cCa) gT*(m^2)*(h)*(V-ET(cCa))
```

```
Rgas    = 831441    % J/(mol*K)
cels    = 36       % K
TK      = 27315    % K
FARADAY = 96489    % C/kmol
cCa0    = 2        % mM
gT      = 22       % mS    (TC=2, RE=175  user: RE=23, TC=22)
Qm      = 5
Qh      = 3
```

```
ET = @(cCa) (1000*(Rgas*(TK+cels))/(2*FARADAY))*log(cCa0/cCa)
minf = @(V) 1/(1+exp(-(V+52)/74))
mtau = @(V) (3+1/(exp((V+27)/10) + exp(-(V+102)/15)))/(Qm^((cels-24)/10))
hinf = @(V) 1/(1+exp((V+80)/5))
htau = @(V) (85 + 1/(exp((V+48)/4) + exp(-(V+407)/50)))/(Qh^((cels-24)/10))
```

```
ODE{end+1,1} = (minf(V)-mT)/mtau(V) % d(m)/dt
ODE{end+1,1} = (hinf(V)-hT)/htau(V) % d(h)/dt
```

iKCa

```
iKCa = @(V,m) Tad * gKCa * m * (V-EKCa)
```

```
gKCa    = 3
EKCa    = -90
Ra      = 01
Rb      = 02
cels    = 36
Q       = 23
caix    = 1
Tad     = (Q)^((cels-23)/10)
```

```
minf = @(cCa) (Ra*cCa) / (Ra*cCa + Rb)
mtau = @(cCa) (1/(Ra*cCa + Rb))/Tad
```

```
ODE{end+1,1} = -(1/mtau(cCa))*(mKCa - minf(cCa))
```

[Ca]i

```
FARADAY = 96489    % C/kmol
depth   = 1E-6     % um, depth of shell
taur    = 5        % ms, rate of calcium removal
cainf   = 24e-4    % mM
```

```
drive = @(x) max( -(10/(2*FARADAY))*x/depth, 0)
```

```
ODE{end+1,1} = drive(SegID_iT_IT(V,mT,hT,cCa)) + (cainf - cCa) /
taur % d([Ca]i)/dt
```

iA

```
iA = @(V,m,h) gA*m^4*h*(V - EK)
```

```
cels = 36
EK = -95
gA = 1 % 2
Tad = 3^((cels-235)/10)
```

```
minf = @(V) 1 / (1+exp(-(V+60)/85))
mtau = @(V) (1/(exp((V+3582)/1969)+exp(-(V+7969)/127) ) +37) /
Tad
hinf = @(V) 1/(1+exp((V+78)/6))
htau = @(V) (V<-63)*(1/(exp((V+4605)/5)+exp(-(V+2384)/3745))) /
Tad + (V>=-63)*(19/Tad)
```

```
ODE{end+1,1} = -(1/mtau(V))*(mA - minf(V)) % d(mA)/dt
ODE{end+1,1} = -(1/htau(V))*(hA - hinf(V)) % d(hA)/dt
```

iCa

```
iCa = @(V,m,h) mphi*gCa*(m^2)*(h)*(V-ECa)
```

```
gCa = 03
ECa = 140
cels = 36
ca0 = 2
Qh = 23
Qm = 23
mphi = (Qm)^((cels-23)/10)
hphi = (Qh)^((cels-23)/10)
```

```
a1 = @(V) 055*(-27-V)/(exp((-27-V)/38)-1)
b1 = @(V) 94*exp((-75-V)/17)
minf = @(V) a1(V) / (a1(V) + b1(V))
mtau = @(V) (1/(a1(V)+b1(V)))/mphi
a2 = @(V) 000457*exp((-13-V)/50)
b2 = @(V) 0065/(exp((-V-15)/28)+1)
hinf = @(V) a2(V) / (a2(V) + b2(V))
htau = @(V) (1/(a2(V)+b2(V)))/hphi
```

```
ODE{end+1,1} = -(mCa - minf(V))/mtau(V) % d(mCa)/dt
ODE{end+1,1} = -(hCa - hinf(V))/htau(V) % d(hCa)/dt
```

ih

```
ih = @(V,o1,o2) gh*(o1+ginc*o2)*(V-Eh)
```

```

k4      = 001
Eh      = -40
cels    = 36
k2      = 0004
nca     = 4
nexp    = 1
taum    = 20

gh      = 02      % 2e-5, mho/cm2
ginc    = 15      % 2
cac     = 0015   % 002
pc      = 01
tadj    = 3^((cels-36)/10)

hinf    = @(V) 1/(1+exp((V+75)/55))
taus    = @(V) (taum + 1000 / (exp((V+715)/142) + exp(-(V+89)/116)
))/tadj
alpha   = @(V) hinf(V)/taus(V)
beta    = @(V) (1-hinf(V))/taus(V)
p10     = @(cCa) 1/(1 + (cac/cCa)^nca)
o10     = @(V,cCa) 1/(1 + (beta(V)/alpha(V)) + (p10(cCa)/pc)^nexp)
o20     = @(V,cCa) (p10(cCa)/pc)^nexp * o10(V,cCa)
klca    = @(cCa) k2 * (cCa/cac)^nca
k3p     = @(p1) k4 * (p1/pc)^nexp

ODE{end+1,1} = alpha(V)*(1-o1-o2) - beta(V)*o1      % d(o1)/dt
ODE{end+1,1} = k3p(p1)*o1 - k4*o2                  % d(o2)/dt
ODE{end+1,1} = klca(cCa)*(1-p1) - k2*p1           % d(p1)/dt

                                iKm

iKm     = @(V,m) Tad*gKm*m*(V-EKm)

EKm     = -90
gKm     = 01
cels    = 36
Q       = 23
qa      = 9
tha     = -30
Ra      = 001
Rb      = 001
Tad     = (Q)^((cels-23)/10)

aa      = @(V) Ra * (V-tha) / (1 - exp(-(V-tha)/qa))
bb      = @(V) -Rb * (V-tha) / (1 - exp((V-tha)/qa))
minf    = @(V) aa(V) / (aa(V) + bb(V))
mtau    = @(V) (1/(aa(V)+bb(V)))/Tad

ODE{end+1,1} = -(1/mtau(V))*(mKm - minf(V)) % d(m)/dt

```

iK (fast)

```

iK      = @(V,n) (Tad*gKv*n)*(V-EKv)

```

```

EKv = -90
gKv = 200%150
Q = 23
tha = 25
qa = 9
Ra = 02
Rb = 002
cels = 36
Vtr = -50
Vtrk = -50
Tad = (Q)^((cels-23)/10)

aa = @(V) Ra*(V-tha)/(1-exp(-(V-tha)/qa))
bb = @(V) -Rb*(V-tha)/(1-exp((V-tha)/qa))
ntau = @(V) (1/(aa(V)+bb(V)))/Tad
ninf = @(V) aa(V)/(aa(V)+bb(V))

ODE{end+1,1} = -(nKv-ninf(V))/ntau(V) % d(n)/dt

```

iNa (fast)

```

INa = @(V,m,h) (mphi*gNa*m^3*h)*(V-ENa)

```

```

Shift = -10
Qm = 23
Qh = 23
tha = -35
qa = 9
Ra = 182
Rb = 124
thi1 = -50
thi2 = -75
qi2 = 5
thinf = -65
qinf = 62
Rg = 0091
Rd = 024
cels = 36
gNa = 3000
mphi = (Qm)^((cels-23)/10)
hphi = (Qh)^((cels-23)/10)
ENa = 50
gNa = 100

```

```

trap0 = @(V,th,a,q) ((V/th)>1E-6)*(a*(V-th)/(1-exp(-(V-th)/q))) +
((V/th)<=1E-6)*(a*q)
mtau = @(V) (1/(trap0(V+Shift,tha,Ra,qa) + trap0(-V-Shift,-
tha,Rb,qa)))/mphi
minf = @(V) trap0(V+Shift,tha,Ra,qa) / (trap0(V+Shift,tha,Ra,qa)
+ trap0(-V-Shift,-tha,Rb,qa))
htau = @(V) (1/(trap0(V+Shift,thi1,Rd,qi2) + trap0(-V-Shift,-
thi2,Rg,qi2)))/mphi
hinf = @(V) 1/(1+exp(((V+Shift)-thinf)/qinf))

```

```
ODE{end+1,1} = -(mNav-minf(V))/mtau(V) % d(m)/dt
ODE{end+1,1} = -(hNav-hinf(V))/htau(V) % d(h)/dt
```

iNaK

```
iNa = @(V,m,h) gNa*(m^3)*(h)*(V-ENa)
iK = @(V,n) gK*(n^4)*(V-EK)
```

```
EK = -95
ENa = 50
gK = 10
gNa = 100
Vtr = -50
Vtk = -50
cels = 36
phi = 3^((cels-36)/10)
```

```
alpha1 = @(V) 32*(13-(V-Vtr))/(exp((13-(V-Vtr))/4)-1)
beta1 = @(V) 28*((V-Vtr)-40)/(exp((V-Vtr)-40)/5)-1)
mtau = @(V) 1/(alpha1(V)+beta1(V))/phi
minf = @(V) alpha1(V)/(alpha1(V)+beta1(V))
alpha2 = @(V) 128*exp((17-(V-Vtr))/18)
beta2 = @(V) 4/(exp((40-(V-Vtr))/5)+1)
htau = @(V) 1/(alpha2(V)+beta2(V))/phi
hinf = @(V) alpha2(V)/(alpha2(V)+beta2(V))
alpha3 = @(V) 032*(15-(V-Vtk))/(exp((15-(V-Vtk))/5)-1)
beta3 = @(V) 5*exp((10-(V-Vtk))/40)
ntau = @(V) 1/(alpha3(V)+beta3(V))/phi
ninf = @(V) alpha3(V)/(alpha3(V)+beta3(V))
```

```
ODE{end+1,1} = -(mHH-minf(V))/mtau(V) % d(m)/dt
ODE{end+1,1} = -(hHH-hinf(V))/htau(V) % d(h)/dt
ODE{end+1,1} = -(nHH-ninf(V))/ntau(V) % d(n)/dt
```

iNa(p)

```
iNap = @(V,m) gNap * m * (V-ENa)
```

```
gNap = 2
Tet = -42
Sig = 5
fNap = 02
cels = 36
Q10 = 27
mphi = (Q10)^((cels-22)/10)
mtau = 8 / mphi
ENa = 50
```

```
minf = @(V) fNap / (1 + exp(-(V-Tet)/Sig))
```

```
ODE{end+1,1} = -(mNap-minf(V))/mtau % d(m)/dt
```